Solar Energy Materials and Solar Cells 200 (2019) 109986

Contents lists available at ScienceDirect

Solar Energy Materials and Solar Cells

journal homepage: www.elsevier.com/locate/solmat

Water-suspended MoO_3 nanoparticles prepared by LASIS and fast processing as thin film by ultrasonic spray deposition

Anderson E.X. Gavim[a], Mariana Richelle Pereira da Cunha[b], Edna Regina Spada[b], Thiago Neves Machado[c], Fabio Seiti Hadano[a], Arandi Ginane Bezerra Jr.[c], Wido Herwig Schreiner[c], Paula Cristina Rodrigues[d], Abd Rashid bin Mohd Yusoff[e], Andreia Gerniski Macedo[c,*], Roberto Mendonça Faria[b], Wilson José da Silva[a]

[a] CPGEI, Federal University of Technology, Curitiba, PR, Brazil
[b] Institute of Physics, University of São Paulo, São Carlos, SP, Brazil
[c] Graduate Program in Physics and Astronomy, Federal University of Technology, Curitiba, PR, Brazil
[d] Graduate Program in Chemistry, Federal University of Technology, Curitiba, PR, Brazil
[e] Department of Physics, Vivian Tower, Singleton Park, Swansea, SA2 8PP, United Kingdom

ARTICLE INFO

Keywords:
Nanoparticles
MoO_3
LASIS
Ultrasonic
Deposition
HIL

ABSTRACT

Crystalline molybdenum oxide nanoparticles (MoO_3 NPs) were prepared by laser ablation synthesis in solution (LASiS). The resulting MoO_3 NPs are water suspended with average size of 23 nm. Subsequently, in order to produce hole injection layers for solar cells, these nanoparticles were processed as thin films onto indium tin oxide (ITO)/glass substrate using ultrasonic spray deposition, which allows fast and uniform deposition in large areas with controllable thickness and low roughness; the water is removed by heating the substrate during the processing. Moreover, scanning electronic microscopy images pointed out that the bottom of the films is mainly composed of small nanoparticles. Thereafter, the optimized glass/ITO/MoO_3NPs/PTB7:PC_{71}BM/Ca/Al solar cells displayed open circuit voltage (V_{oc}) of 0.75 V, short circuit current density (J_{sc}) of 13 mA/cm^2, fill factor (FF) of 58% and power conversion efficiency of 5.7% under AM1.5 illumination, presenting increased stability when compared with devices having polymeric hole transporting layer. Since LASiS method does not require the use of organic precursors/solvents, it is a green route to produce MoO_3 NPs. In addition, the ultrasonic spray deposition is a versatile method to achieve homogeneous and transparent thin films from water suspended nanoparticles. The organic solar cell response pointed out the potential use of these procedures to produce hole injection layers for photovoltaic devices.

1. Introduction

Several conjugated molecules and copolymers have been applied as active layer in solution processed organic solar cells (OSCs), reaching power conversion efficiencies (PCE) at the range of 13% from non-fullerene based cells [1] and 17.3% from tandem cells [2]. Major limitations for scale up production are related with the difficult processing in large areas and the low stability of conjugated materials in ambient atmosphere. To avoid these issues, researchers have focused on new processing techniques such as roll-to-roll [3], soft embossing [4], spray [5] and ultrasonic deposition [7,8]. Moreover, spray combined with ultrasonic deposition is a versatile and low cost method that allows the processing of thin films with controlled thickness/roughness by optimization of parameters such as concentration of the solution/suspension, time of deposition and temperature [7,8]. This method has been used to process buffer layers, active layers and perovskites for solar cells [7–11]. In OSCs the use of anode buffer layer (ABL), commonly referred as hole transporting layer (HTL) or hole injection layer (HIL), is a strategic procedure to avoid the leaking of electrons to the ITO electrode and improvement of the anode electrode efficiency in collecting/injecting positive carriers, respectively. To work as an efficient ABL the film must be transparent, insoluble in organic solvents, as well as displays low roughness, good mechanical and proper transport properties [12,13]. Furthermore, in order to avoid the use of poly(3,4-ethylenedioxythiophene)-poly(styrenesulfonate) (PEDOT:PSS) as HTL, due its acid character, other materials have been tested such as vanadium oxide (VO_x) [5], molybdenum oxide (MoO_3) [7,8] and graphene oxide [14], the reason being to the increased stability of the resulting

* Corresponding author.
E-mail address: agmacedo@utfpr.edu.br (A.G. Macedo).

https://doi.org/10.1016/j.solmat.2019.109986
Received 11 February 2019; Received in revised form 27 May 2019; Accepted 6 June 2019
Available online 13 June 2019

devices [15] when compared with acidic PEDOT:PSS based OSCs. Also, the films produced with these oxides have the advantage of being water compatible which allows the sequential processing of water based donor:acceptor inks used as active layer [10].

Specifically, MoO_3 HIL reduces charge recombination and resistance at the interface of photoactive layer and anode. For instance, C. Dwivedi et al. [6] reported MoO_3 films prepared using spray pyrolysis and ammonium heptamolybdate as precursor in water, with the substrate at temperatures of 500–800 °C. The resulting work function of MoO_3 was 5.1 eV measured by Kelvin probe. The performance as HIL of these MoO_3 films was compared with thermally evaporated MoO_3 having poly({4,8-bis[(2-ethylhexyl)oxy]benzo[1,2-b:4,5-b′]dithiophene-2,6-diyl}{3-fluoro-2-[(2-ethylhexyl)carbonyl]thieno[3,4-b]thiophenediyl}):phenyl-C_{71}-butyricacidmethylester (PTB7:$PC_{71}BM$) as active layer, the devices resulted in comparable PCE values of 2.7% and 2.96%, respectively. N. Chaturverdi et al. [7] reported the preparation of MoO_3 HIL with electric field assisted spray deposition using heptamolybdate tetrahydrate as precursor in water, substrate at 400 °C and applying voltages of 0.5 kV and 1 kV. The results pointed out that deposition performed at 400 °C resulted in uniform films with thickness of 25 nm. OSCs having poly(3-hexylthiophene) [6,6]:-phenylC_{61}-butyricacidmethylester (P3HT:$PC_{61}BM$) as active layer were produced with MoO_3 HIL deposited by electric field assisted spray deposition (1 kV) and compared with OSCs having MoO_3 HIL deposited by spin coating. Photovoltaic characterization showed that these devices have similar performance, resulting in PCEs of 2.71% and 2.51%, respectively. Kelvin probe analyses showed a slight increase on the work function of MoO_3 by applying voltages from 4.9 eV to 5.0 eV. This feature may enhance hole transport between the active layer and the (indium tin oxide) ITO electrode. Inverted OSCs were produced with MoO_3 arrays deposited by ultrasonic spray coating onto the P3HT:$PC_{61}BM$ active layer [8]. In this case, the ammonium heptamolybdate in water:alcohol solution was used as precursor for MoO_3 compound while the substrate was heated at 80 °C. The multicomponent solvent system enhanced MoO_3 film morphology and the OSCs showed the highest PCE of 3.4%. This value is similar to the PCE value of OSCs produced with thermally evaporated MoO_3 (PCE = 3.23%).

In another approach, vanadium triisopropoxide was used as precursor for VO_x films produced by electrospray deposition [5]. Improved photovoltaic device performance was achieved with the ITO/VO_x anode in OSCs devices with PTB7:$PC_{71}BM$ active layers resulting in a PCE of 7.3%. This improvement was attributed to the smooth surface texture and favorable chemical composition with higher hole mobility of VO_x produced by electrospray deposition. Synthesized nanoparticles suspensions have also been processed by ultrasonic spray deposition for production of electrochromic devices based on tungsten oxide (WO_3) NPs [16], silver top electrodes in OSCs [17], among others.

Herein, crystalline molybdenum oxide nanoparticles (MoO_3 NPs) were synthesized through laser ablation synthesis in liquid solution (LASiS), also known as laser ablation in liquids (LAL) [18,19], which is considered a physicochemical combined *top-down* and *bottom-up* method. One of its main advantages over other methods resides in nanoparticles production in pure liquids without the aid of stabilizing molecules. In short, a laser pulse interacts with a target immersed in liquid, thus generating a plasma plume on the target surface. This plasma is composed of highly ionized or atomic species and as the plume abruptly collapses, it leads to nanoparticles formation [18,19]. Generally, laser ablation in water leads to oxidized nanoparticles and the process produces defects in the synthesized colloids which are essential to provide surface charge and thus electrostatic stabilization. The resulting MoO_3 NPs were processed as thin films onto ITO/glass substrates using ultrasonic spray deposition upon temperatures at the range of 80 °C–150 °C. The performance of the MoO_3 NPs as HIL in OSCs was also evaluated.

2. Experimental

Materials: PEDOT:PSS (1000 S/cm, Baytron®), PTB7 (Solarmer) and $PC_{71}BM$ (American Dye Source, Inc).

2.1. Preparation of water suspended MoO_3 NPs

MoO_3 NPs were prepared using a Q-switched Quantronix Model 117 Nd:YAG laser (1064 nm), operating at 1.5 kHz and delivering 200 ns pulses at the fundamental harmonic. The laser beam was focused with a 50 mm lens on a molybdenum target (Williams Advanced Materials, 5 N), producing a 40-μm spot size. The laser power was set at 9×10^5 J/m^2. The target was placed 3 mm under bidistilled water and the total water amount was maintained at 15 ml. The irradiation time was of 5 min, and the process was repeated four times under the same experimental conditions to yield a total colloidal volume of 60 ml.

The optical characterization of nanoparticle colloids was performed with an Ocean Optics Model USB2000 + spectrometer in the range from 200 to 1000 nm with 2 nm resolution. Dynamic light scattering (DLS) with a Microtrac Nanotrac Ultra model was used for hydrodynamic particle size determination. Transmission electron micrographs (TEM) were obtained on a JEOL JEM1200EX-II, operating at 120 kV, using Formvar/Carbon mesh 200 Cu grid substrates, in which drops of the nanoparticle suspension were deposited and let to dry. Selected area electron diffraction (SAED) was employed to crystal structure determination with the same apparatus used for TEM. Raman scattering spectra were obtained with a confocal Raman Alpha 300R microscope from WiTec. Laser excitation at 532 nm was employed to check Raman scattering response. Only freshly prepared nanoparticles were used.

XPS (X-ray photoelectron spectroscopy) measurements were performed using a VG Microtech ESCA 300 system with an Al X-ray anode, a 250 mm semi-hemispherical energy analyser, 9 channel detectors and a base vacuum of 3×10^{-10} mbar. The system energy resolution was 0.8 eV. Binding energy referencing was done using C-1s binding energy of 284.5 eV [20]. A 1 ml drop of the LASiS synthesized molybdenum colloidal suspension was placed on the surface of a Si wafer and let to dry. The resulting film was introduced in the XPS vacuum chamber for analysis.

2.2. Thin film deposition of MoO_3 nanoparticles using ultrasonic spray

The deposition of MoO_3 HIL was carried out using an ultrasonic spray coating system (Scheme 1). The as synthesized MoO_3 NPs suspension was diluted in ultrapure water (1:8 v/v) upon ultrasonic stirring during 5 min at room temperature. In this work, the nozzle remained in a fixed position, placed about 0.3 cm over the heated substrate at temperature range of 80 °C–150 °C and spray area of ~9 cm^2. Both suspension volume and deposition rate can be adjusted in accordance with the size of the substrate. Moreover, the setup allows mechanical translation movement in a plane parallel to the substrate or, in the case of flexible substrates; these can be dislocated, with a proper velocity, using a roll-to-roll system (R2R) coupled to a heater, these studies are underway. Fig. S1 shows a schematic representation of the spray deposition coupled to R2R system and an image of MoO_3 NPs spray deposited onto PET/ITO substrate, while it was horizontally moved and heated by the R2R system. In order to process the MoO_3 NPs HIL onto the glass/ITO substrate, 4 mL of this suspension was placed into the ultrasonic vessel, then injected into the spray nozzle at 0.5 ml/min under 1.7 MHz for 40–100 s. After, the flow of MoO_3 NPs was interrupted and the substrate remained heated during 120 s for residual water removal. Topography was analysed by scanning electronic microscopy (SEM), atomic force microscopy (AFM) and cross section profiles which were performed along the surface. SEM images were acquired using a Zeiss Sigma field emission SEM equipment operating at 2 kV and work distance of 8.5 mm. Topography and phase images

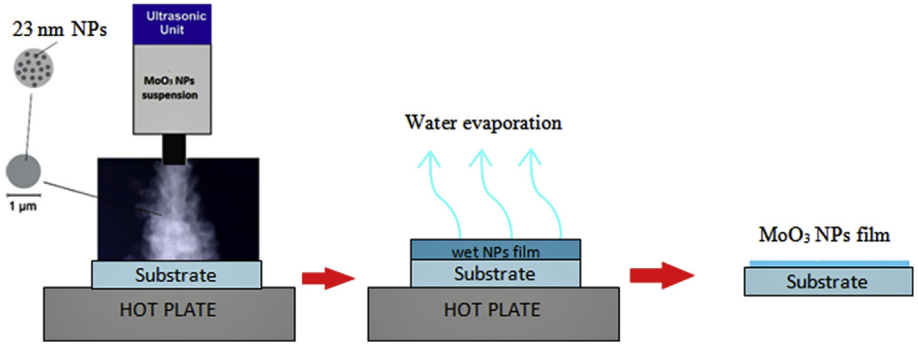

Scheme 1. Ultrasonic spray deposition from water suspended MoO_3 NPs.

were acquired by using an AFM Shimadzu SPM-9700 operating in dynamic mode using a silicon tip with frequency of 285 kHz and force constant of 42 N/m (arrowNCR-10 from Nano World). Additional topography, thickness and roughness measurements were performed using a 3D optical surface profiler (Taylor Hobson) and/or a Dektak profilometer. The resulting MoO_3 film has thickness between 5 and 20 nm and root mean square roughness (R_{rms}) of 4 ± 2 nm.

2.3. Production of photovoltaic devices

In order to evaluate the performance of MoO_3 NPs HIL in bulk heterojunction OSCs, this material was processed as thin film onto cleaned and pre-patterned glass substrate coated with a thin layer of ITO (8–12 Ω/sq, thickness 120 nm, Delta Technologies), though a shadow mask using the procedure described above. Prior the deposition of MoO_3 NPs, the glass/ITO substrate was cleaned with sequential washing in ultrapure water, Extran, acetone and isopropyl alcohol [21]. Further, the active layer composed of PTB7:PC_{71}BM (1:1.5, 20 mg/mL in chlorobenzene, 3% v/v 1,8-diiodooctane) was deposited onto the glass/ITO/MoO_3NPs by spin coating at 700 rpm during 30 s followed by 2100 rpm during 60 s or 1000 rpm during 60 s, at room temperature under inert atmosphere; these PTB7:PC_{71}BM films exhibited thickness of about 80 nm and 110 nm respectively. Sequentially, the active layer was washed with 100 µL of anhydrous methanol upon 4000 rpm during 40 s. Finally, the anode composed of Ca (15 nm) and Al (70 nm) was deposited by thermal evaporation. The area of the device was of 4.5 mm^2. Moreover, a reference device (without HIL or HTL) and a similar device, in which PEDOT:PSS film acts as HTL, were built for terms of efficiency comparison. For this purpose, 30 nm of PEDOT:PSS was deposited by spin coating onto the glass/ITO substrate at 2000 rpm during 60 s and dried at 140 °C during 15 min in vacuum. The device response was evaluated upon illumination of 100 mW/cm^2 using a Solar Simulator Oriel Class AAA coupled to a filter AM 1.5G. The J-V curves were acquired using a Keithley 2400 electrometer.

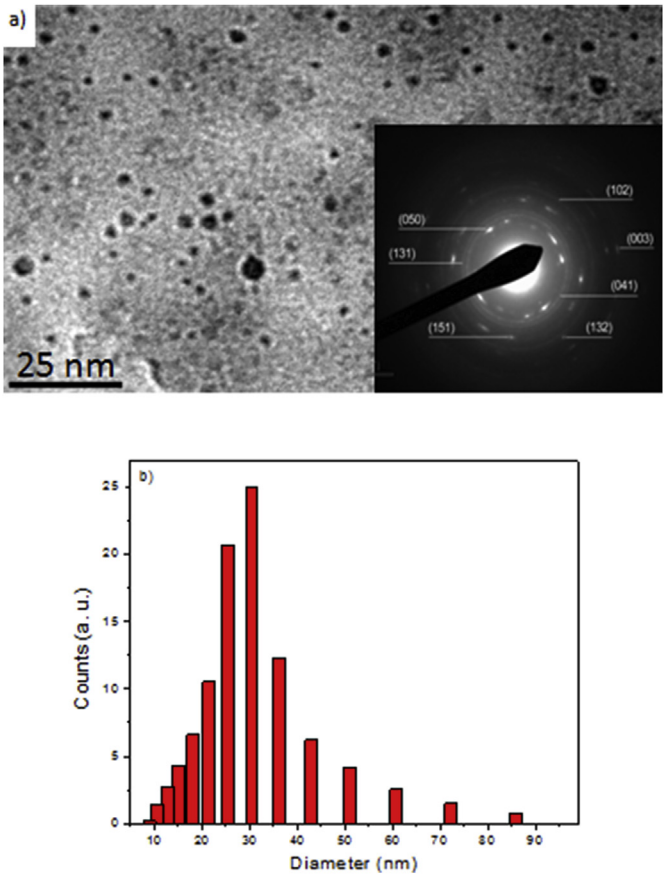

Fig. 1. a) TEM image and SAED pattern acquired from MoO_3 nanoparticles and b) size distribution measured by DLS.

3. Results and discussion

3.1. Synthesis and characterization of the MoO_3 NPs

Size control, low content of impurities and stability are among the issues related with synthesis of nanoparticles in solution [18,19]. Mainly, for application as HIL, these nanoparticles must be chemically stable, display low size distribution and proper optical/electrical properties. Due this, to ensure that the MoO_3 NPs are suitable for application as HIL, several analyses were performed to evaluate these features, the results are presented and discussed as follow.

TEM images were acquired to evaluate the morphology of the MoO_3 NPs, pointing out the presence of small (less than 10 nm), spherical and non aggregated particles from the aqueous colloidal dispersion, Fig. 1a. In addition, SAED pattern is also presented, indicating that these nanoparticles are crystalline, whose phase can be indexed to the orthorhombic phase of MoO_3 [22]. The hydrodynamic diameter measured by DLS is shown at Fig. 1b and corresponds to a relatively broad size dispersion, which is characteristic of most laser ablation nanoparticles production processes [19], with an average diameter of 23 nm.

The stoichiometric composition of the HIL is an important feature for this application because this parameter impacts directly onto the work function and electrical properties [23,24]. To further characterize the chemical features of MoO_3 NPs, Raman and XPS spectra were taken of a dried droplet (1 µL) of the nanoparticles suspension. Fig. 2a displays the vibrational spectrum taken with a 532 nm laser excitation. The peaks at 667, 820 and 995 cm^{-1} are a clear indication of MoO_3, as reported at the literature [25,26]. The stretching frequencies at 995 cm^{-1} and 821 cm^{-1} are attributed to the Mo–O and the intermediate bridging O–Mo–O bonds, respectively. A low intensity shoulder at 667 cm^{-1} may arise from the symmetric stretching vibration of the

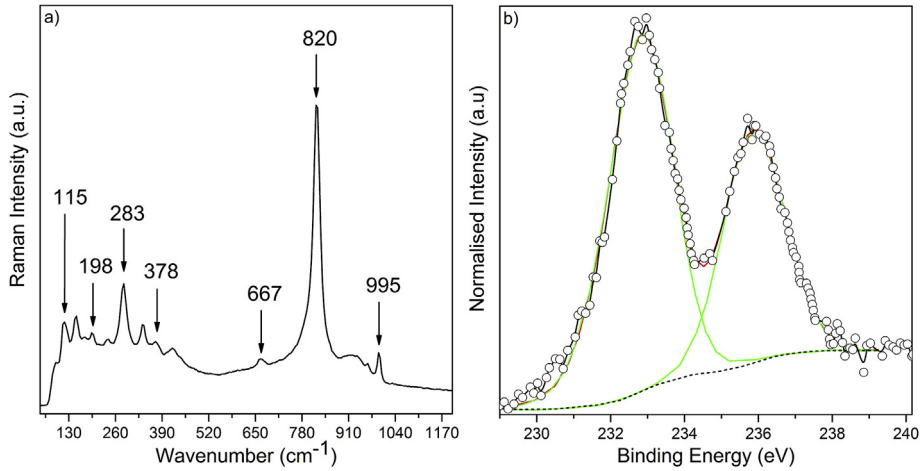

Fig. 2. a) Raman and b) high resolution XPS spectrum of Mo 3d binding energy region acquired from MoO_3 NPs film produced by drop casting method.

bridging O–Mo–O along the (001) lattice direction. The bending modes are located in the medium frequency range, whereas the external modes appear at below 200 cm^{-1}.

Moreover, XPS regarding Mo 3d spectrum can be fitted by one 3d doublet in the form of a Gaussian function, corresponding to molybdenum with a single oxidation state. These results are shown in Fig. 2b. The $3d_{5/2}$ level at 232.9 eV and $3d_{3/2}$ peak centred at 236.0 eV are typical values of 3d doublet of Mo^{6+}, indicating that the particles present the MoO_3 phase [27–29], which corresponds to the more stable oxide phase of this element. This record is in accordance with the SAED and RAMAN results presented at Figs. 1a and 2a, respectively.

UV–Vis absorbance/transmittance an diffuse reflection analyses were performed to obtain the band-gap energy of the MoO_3 NPs. For comparison purposes the absorbance spectra acquired from MoO_3 NPs in water and thin films are presented at Fig. 3. The absorbance spectra o MoO_3 films exhibits absorption bands at 193 and 230 nm; a shoulder is also observed at 325 nm which corresponds to a surface plasmon resonance of Mo [30]. The optical band gap was evaluated from the Tauc-plot [6] presented at the inset of Fig. 3. Calculated band gap value is found to be 3.4 eV, this value is in accordance with those reported for MoO_3 nanostructures [7], which is blue-shifted when compared with to that of bulk MoO_3 (~2.9 eV) [31]. This shift has been attributed to the nanostructured nature of the films, where charges are localized in individual nanocrystals, which results in increased band gap energy [32]. MoO_3 film acts as electron extractor or hole injector material, in OSCs this function is determined by the relative energy position at the junction [33]. In this work, the MoO_3 NPs electrode acts as hole injector material because the work function of 5.1 eV promotes the hole injection at the active layer. Wider band gap in MoO_3 electrodes is beneficial to its action as buffer layer in OSCs, since it will reduces the energy barrier for hole injection/extraction between the active layer and ITO electrode [33]. Considering the AM1.5G spectrum, there is minor contribution of photons at the wavelength around 3.4 eV (~360 nm); therefore, the MoO_3 film does not contribute to the generation of photocurrent. However, its high transmittance at the visible range (83–89%) allows proper performance as HIL and creation of excitons at the PTB7:PC_{71}BM active layer.

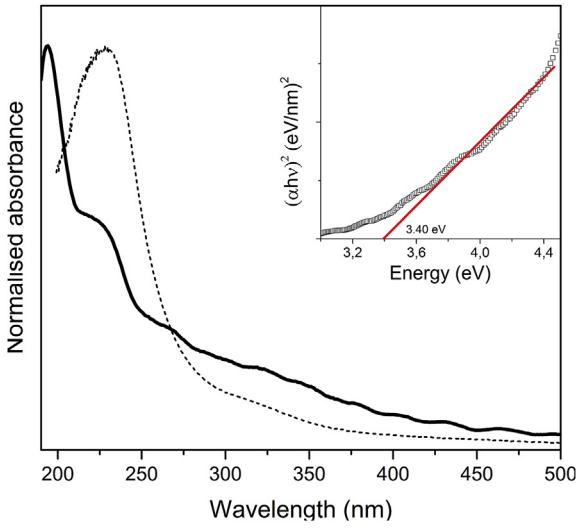

Fig. 3. UV–Vis absorbance spectra of MoO_3 nanoparticles synthesized by laser ablation in water (dotted line) and film (solid line). Inset: Tauc plot used to determine the energy band gap.

3.2. Processing MoO_3 NPs as thin film by ultrasonic spray deposition

Prior the testing as HIL, the MoO_3 layer was optimized by the changes in parameters such as concentration, time and temperature during the ultrasonic spray deposition. It was found that the as prepared MoO_3 NPs suspension is high concentrated and, due this, the mist is not formed at the frequency range of the ultrasonic equipment. This problem was overcome by diluting the initial NPs suspension in ultrapure water at the ratio 1:8 (v/v).

MoO_3 NPs films deposited onto glass substrate were analysed by SEM and optical profilometer, these images are presented at Figs. 4 and S2, respectively. The results pointed out that both time and temperature have influence on the resulting morphology, for instance: films produced at temperature range of 80–150 °C and short time of deposition (~40–60 s) presented uniform covering; while the films produced at temperature range of 100–150 °C and longer times (> 60 s) were not homogeneous, presenting cracks or aggregates of NPs along the surface. Therefore, time and temperature parameters must be controlled in order to achieve high-quality MoO_3 NPs films. In order to ensure the homogeneity, films produced onto substrates with dimensions of 1.5 cm × 2.5 cm were analysed at the centre and lateral regions, the results showed that the deposition is uniform over the substrate surface (Fig. S3). Considering the application as HIL in OSCs, the films produced substrate heated at 80–120 °C during 40–60 s presented proper covering, thickness and low roughness, being suitable to be used as HIL in OSCs. AFM image acquired from MoO_3 NPs film is shown at Fig. 5, where the corresponding phase image confirms the uniform distribution of the spherical particles onto the substrate. Cross section profiles acquired using Dektak, optical profilometer and AFM methods were also compared, these profiles showed that this film is formed by particles with height ranging from 5 to 20 nm, being predominantly sub-10 nm

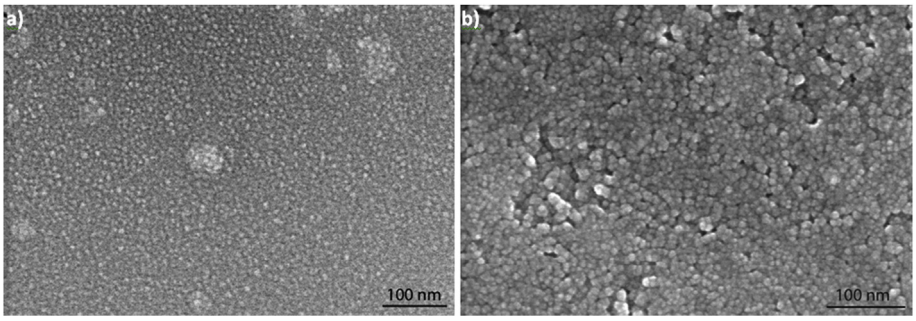

Fig. 4. SEM images acquired from MoO_3 NPs films produced onto substrate heated at 120 °C and deposition times of a) 40 s and b) 60 s (magnification 200 kx).

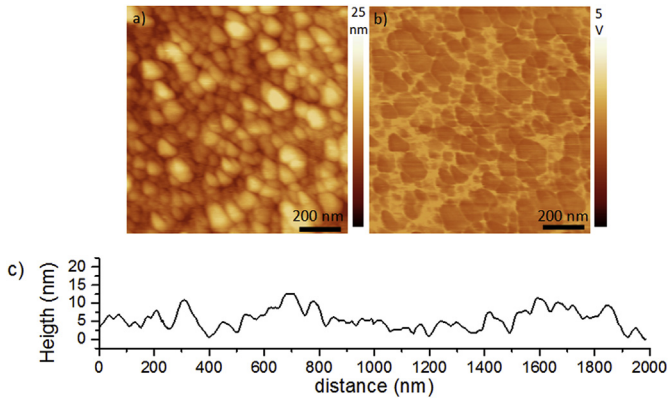

Fig. 5. a) Height, b) phase AFM images and c) cross section profile acquired from MoO_3 NPs film produced by ultrasonic spray deposition (60 s) with the substrate heated at 120 °C.

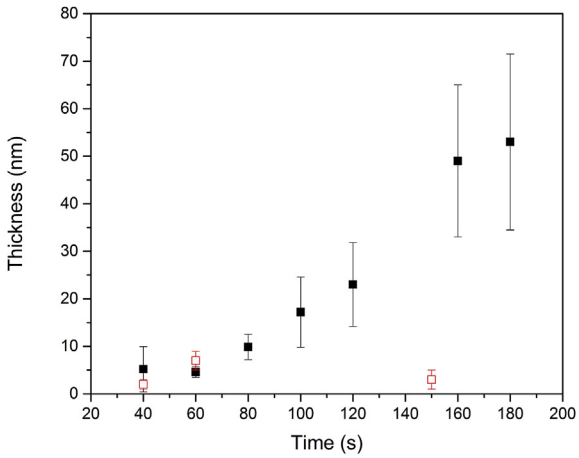

Fig. 6. Thickness versus time of ultrasonic spray deposition with substrate heated at (□) 80 °C and (■) 120 °C.

sized (Fig. S4). This outcome, when compared with the size distribution result presented at Fig. 1b, point out that the initial mild flux is formed mainly by small particles, this selectivity results in films with variable grain size along the thickness and higher roughness when adopting longer times of ultrasonic deposition [34]. This can be also verified at Fig. 4, which shows the comparison between the MoO_3 NPs films produced at times of 40 s and 60 s, while Fig. 6 presents the thickness versus time of deposition with the substrate heated at 80 °C and 120 °C. Films produced at 80 °C presented average thickness from 2 to 7 nm (R_{rms} = 0.6–2.5 nm), while at 120 °C the thickness increases from ~5 nm up to ~ 53 nm (R_{rms} = 2–6 nm) when the time of deposition changes from 40 s to 180 s, respectively. Since MoO_3 are multifunctional materials, besides the HIL function, thicker films can be used in other optoelectronic devices. For instance, MoO_3 films have been used as sensing layers in biosensors, S. Balendhran et al. [35] used nanostructured MoO_3 films with thickness between 80 and 220 nm in field effect platform to monitor the effect of Coulombic charges using bovine serum albumin (BSA).

3.3. Evaluation of MoO_3 NPs as hole injection layer in organic solar cells

Previous reports about MoO_3 films thickness effect on photovoltaic response of organic solar cells pointed out that the that only 1 nm-thick MoO_3 is enough to exhibit highly efficient devices and that increasing the thickness up to 15–20 nm does not change the device performance [36,37]. However, devices prepared with MoO_3 films with thickness higher than 15–20 nm showed decrease of J_{sc} and FF parameters, resulting in lower power conversion efficiency. Moreover, in order to evaluate the electrical properties of MoO_3 NPs film, the *J-V* curve was acquired from ITO/MoO_3 NPs (120 nm)/ITO device (Fig. S5); the calculated resistance value is ~17 MΩ, which is lower than those reported for MoO_3 film produced by spray deposition ($R = 45 \times 10^9\ \Omega$) [38] and at same order of values reported for MoO_3 film (150 nm) [39] and MoO_3 film produced by sol-gel method [40]. Therefore, as described previously and to avoid increase the series resistance at the OSC [41], the MoO_3 NPS films prepared upon ultrasonic deposition during 40–60 s at 80 °C–120 °C were chosen to be tested as HIL.

Scheme 2 shows the energy level diagram and the sequence of layers at the OSC produced with MoO_3 NPs as HIL. In order to understand the role of MoO_3 as hole injection layer, in accordance with M. Kröger et al. [42] and J. Meyer et al. [43,44], the Fermi level is pinned against the conduction band minimum due to oxygen vacancy defects, indicating a n-type material. Therefore, due the low energy barrier between the MoO_3/PTB7 (< 0.5 eV), the injection of holes from ITO to the organic semiconductor layer results from electron extraction from P7B7 HOMO through the MoO_3 conduction band, and then into ITO, instead of hole transit from ITO through the MoO_3 valence band. The MoO_3 reduces the energy barrier for negative charge extraction between the ITO and the HOMO level of active layer and thus, enhancing the hole injection.

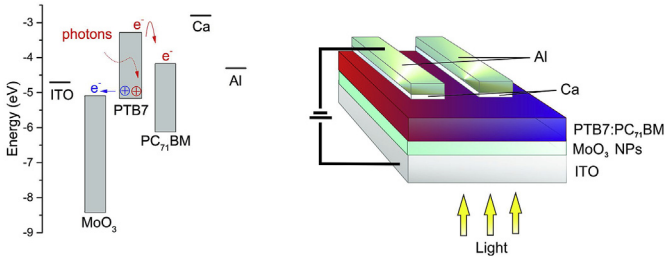

Scheme 2. Energy level diagram and structure of ITO/MoO_3NPs/PTB7:PC_{71}BM/Ca/Al device, where PTB7 and PC_{71}BM act as electron donor and acceptor, respectively. At the energy level diagram the blue color denotes the electron extracted from P7B7 HOMO to the MoO_3 conduction band, while the red color denotes the photogenerated electron-hole pair (exciton).

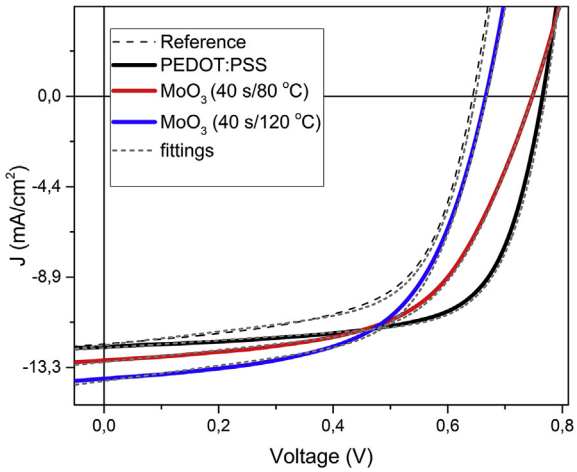

Fig. 7. *J-V* curves measured under AM1.5G illumination from glass/ITO/MoO_3NPs/PTB7:PC_{71}BM/Ca/Al devices. *J-V* curves acquired from devices without HTL or having PEDOT:PSS as HTL are also presented for comparison. The short-dashed lines are theoretical fittings using Equation (1).

Upon illumination through the ITO/MoO_3 transparent electrodes, bounded electron-hole pairs (excitons) are created at the PTB7:PC_{71}BM active layer, migrate along ca. 10 nm and then dissociate. After reaching the interface donor:acceptor, the negative charge is mostly transferred to the Ca–Al electrode through the LUMO level of electron acceptor PC_{71}BM [6].

The OSCs were illuminated through the ITO side and, prior the light achieves the active layer; there is a loss due diffuse reflection (ca. 15%) at the visible range (Fig. S4). However, this loss was considered during the calibration of solar simulator at the intensity of 100 mW/cm^2 performed using a glass plate. *J-V* curves acquired at dark from ITO/MoO_3NPs/PTB7:PC_{71}BM/Ca/Al devices showed diode characteristic behavior with rectification factor of about 10^2, in the −2 to 2V range. Fig. 7 displays similar measurements performed under illumination showing that the device having MoO_3 NPs as HIL exhibits a promising photovoltaic response when compared with the reference device (without HTL) or having PEDOT:PSS as HTL. Table 1 summarizes the photovoltaic parameters obtained from these devices and varying the experimental conditions to produce the MoO_3 NPs film layer. The highest PCE obtained from the MoO_3 device was 5.7% somewhat lower than that exhibited by the device produced with PEDOT:PSS as HTL, which reached 6.4%, but is higher from the reference device, which displayed PCE of 4.8% (see Table 1).

The replacement of PEDOT:PSS as standard HTL by another material, can in principle change the electrical characteristics of the photovoltaic cell, which certainly modifies the values of the series and shunt resistances of the device. To better analyze this exchange effect, adjustments of the *J-V* curves under illumination for all devices here investigated making use of the expression for the equivalent circuit of a solar cell of the heterojunction type [45]:

$$I(V) = I_S\left[\exp\left(\frac{q(V + R_S I)}{nk_B T}\right) - 1\right] + \frac{V + R_S I}{R_{sh}} - I_{ph}(V) \quad (1)$$

In this equation, I_s is the diode reverse saturation current, I_{ph} is the photocurrent, q is the electron charge, R_s is the series resistance, R_{sh} is the shunt resistance, k_B is the Boltzmann constant, T is the temperature, and n is the diode ideality factor. Taking into account that the bimolecular recombination effect dominates the diffusion process, we assume $n = 2$. Thereby, the only factors used as adjustment parameters are the series and the shunt resistances. The fittings are shown in Fig. 7 and the obtained values for R_s and R_{sh} are shown in Table 1. The results pointed out that the exchange of PEDOT:PSS by MoO_3 causes increases in the value of the series resistance, and reductions in the shunt resistances. In principle both variations were negative for a performance improvement of the devices, but even so the performance of the solar cell with MoO_3 NPs was close to the traditional one built with PEDOT:PSS. That is, when comparing the photovoltaic MoO_3 NPs-device of best performance (5.7%) with that of best performance using PEDOT:PSS (6.4%), there is a 6-fold increase in the series resistance and a 58% reduction in the shunt resistance. This indicates that the next steps should then focus on decreasing the series resistance and increasing the shunt one, and thereby moving toward the goal of obtaining more efficient cells than traditional ones with PEDOT: PSS.

Moreover, PEDOT:PSS has been used for more than a decade as HTL and OSCs produced with MoO_3 films show longer lifetime when compared with devices produced with PEDOT:PSS [46,47] and without HTL, see Fig. 8. The OSC degradation due PEDOT:PSS has been attributed to its hygroscopic and acid character that contribute to reduced stability in air [47] and without HTL there is increased diffusion indium from the ITO electrode into the active layer [48]. Therefore, these MoO_3 NPs have potential for such a function and research in this direction must go forward. Devices produced with thicker MoO_3 NPs, for instance during 60 s and substrate at 120 °C, presented a reduction in the J_{sc}, which can be explained by the appearance of impedance generated at either the ITO/MoO_3 or at MoO_3/PTB7-PC_{71}BM interfaces. Moreover, since the V_{oc} value is mostly defined by the work functions of the electrodes and by the difference between the lowest unoccupied molecular orbital (LUMO) of the PCBM and the highest occupied molecular orbital (HOMO) of the PTB7, the reduction of V_{oc} in these devices may be related with diffusion of MoO_3 nanoparticles inside the active layer, which is not ruled out, or due the influence of higher roughness of MoO_3 NPs films ($R_{rms} = 4 \pm 2$ nm) than that of PEDOT:PSS films ($R_{rms} = 1 \pm 0.3$ nm), these features can influence the energies of positive and negative charge carriers. Similar reduction on V_{oc} was reported for OSC having solution processed MoO_3 films ($R_{rms} = 3$ nm) as HIL and poly-hexylthiophene:indene-C60 bisadduct (P3HT:ICBA) as active layer [46]. Moreover, the OSCs having MoO_3 NPs as HIL showed fill factor parameters at the range of 58–60%, that point out low series resistance at the device [49]. Additionally, the resulting PCE of 5.7% is promising when compared with the PCEs reported for OSCs having MoO_3 HIL processed by spray/ultrasonic methods using organic precursors [7,8] and having the same active

Table 1
Photovoltaic parameters obtained from OSCs having MoO_3 NPs HIL deposited by ultrasonic spray or PEDOT:PSS HTL deposited by spin coating, with PTB7:PC_{71}BM as active layer.

Anode Buffer Layer	Thickness PTB7:PC_{71}BM (nm)	V_{OC} (V)	J_{SC} (mA/cm^2)	FF (%)	R_s (Ωcm^2)	R_{sh} (Ωcm^2)	PCE (%)
Reference	110	0.65	12.2	61	1.7	294	4.8
MoO_3 NPs (40 s/80 °C)	110	0.75	13.0	58	6.0	402	5.7
MoO_3 NPs (40 s/120 °C)	110	0.70	13.9	59	2.7	300	5.5
MoO_3 NPs (40 s/150 °C)	110	0.72	12.1	60	3.7	380	5.2
MoO_3 NPs (60 s/120 °C)	110	0.66	11.8	59	2.6	324	4.6
MoO_3 NPs (60 s/120 °C)	80	0.64	9.4	58	2.5	294	3.5
PEDOT:PSS	80	0.76	10.5	63	1.3	373	5.0
PEDOT:PSS	110	0.77	12.3	68	1.1	546	6.4

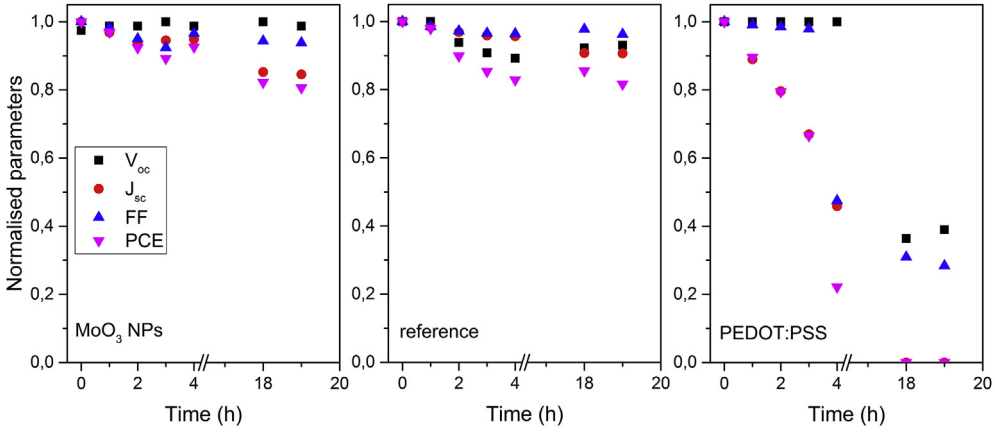

Fig. 8. Normalised photovoltaic parameters acquired from OSC having MoO_3 NPs as HIL, reference (without HTL) and PEDOT:PSS as HTL versus aging time in air.

Table 2
Photovoltaic parameters reported by C. Dwivedi et al. [6].

Anode Buffer Layer	V_{OC} (V)	J_{SC} (mA/cm^2)	FF (%)	PCE (%)	Ref.
CoSP–MoO_3[a]	0.52	15.4	34	2.7	6
e-MoO_3[b]	0.52	13.4	42	2.96	
PEDOT:PSS	0.61	15.0	48	4.4	

[a] MoO_3 film prepared by spray pyrolysis using organic precursor.
[b] Thermally evaporated MoO_3 film.

layer PTB7:PC_{71}BM [6], Table 2. Therefore, it is important to emphasize that the MoO_3 NPs prepared by LASIS have small size distribution (ca. 23 nm); the resulting water suspensions are stable over the aging time, being fast and selectively processed as thin film using the spray ultrasonic deposition at low temperatures. These features avoid the NPs aggregation previously reported in MoO_3 films processed by spin coating [44].

4. Conclusions

In summary, the results demonstrated that MoO_3 NPs, presenting average size distribution of 23 nm in aqueous colloidal suspension, were successfully prepared by LASIS synthesis, which is a green route to produce nanoparticles because circumvent the use of organic precursors/solvents and stabilizing molecules. TEM results pointed out the presence of sub-10 nm sized particles. SAED pattern, XPS and RAMAN results confirmed the crystalline character and the MoO_3 phase. Kelvin probe pointed out that the work function is 5.1 eV; this value allows the use of MoO_3 NPs as hole injection layer with ITO electrode in organic solar cells, providing proper energy alignment to inject holes at the device. The ultrasonic spray deposition method was employed to process uniform thin films in large areas with controllable thickness. The photovoltaic response of glass/ITO/MoO_3NPs/PTB7:PC_{71}BM/Ca/Al pointed out the potential of these procedures to produce HILs for photovoltaic devices.

Acknowledgements

This work was financially supported by Fundação Araucária (grants 327/2014), Fundação Parque Tecnológico Itaipu (FPTI-BR, call FA 21/2018), Conselho Nacional de Desenvolvimento Científico e Tecnológico (CNPq, grants PQ2 308129/2018-0, Equinor 440078/2019-9), Coordenação de Aperfeiçoamento de Pessoal de Nível Superior (CAPES, PVEX 88881.171856/2018–01 and Finance Code 001) and Serrapilheira Institute (grant number Serra-1709-17054). The authors also acknowledge the INEO (Instituto Nacional de Eletrônica Orgânica), LAMAQ-UTFPR by spectroscopy facilities, CME-UFPR and CMME-UTFPR by AFM and SEM facilities, respectively.

Appendix A. Supplementary data

Supplementary data to this article can be found online at https://doi.org/10.1016/j.solmat.2019.109986.

References

[1] J. Hou, O. Inganäs, R.H. Friend, F. Gao, Organic solar cells based on non-fullerene acceptors, Nat. Mater. 17 (2) (2018) 119–128 https://doi.org/10.1038/nmat5063.
[2] L. Meng, Y. Zhang, X. Wan, C. Li, X. Zhang, Y. Wang, X. Ke, Z. Xiao, L. Ding, R. Xia, H.L. Yip, Y. Cao, Y. Chen, Organic and solution-processed tandem solar cells with 17.3% efficiency, Science 361 (2018) 1094–1098 https://doi.org/10.1126/science.aat2612.
[3] A.E.X. Gavim, G.H. Santos, E.H. de Souza, P.C. Rodrigues, J.B. Floriano, R.C. Kamikawachi, J.F. de Deus, A.G. Macedo, Influence of electrolyte distribution in PEDOT:PSS based flexible electrochromic devices, Chem. Phys. Lett. 689 (2017) 212–216 https://doi.org/10.1016/j.cplett.2017.10.022.
[4] R. Meier, C. Birkenstock, C.M. Palumbiny, P.M. Buschbaum, Efficiency-improved organic solar cells based on plasticizer assisted soft embossed PEDOT:PSS layers, Phys. Chem. Chem. Phys. 14 (2012) 15088–15098 https://doi.org/10.1039/C2CP42918G.
[5] H.A. Kavuri, T. Fukuda, K. Takahira, A. Takasashi, S. Kihira, D.J. McGillovray, G. Willmott, Electrospray-deposited vanadium oxide anode interlayers for high-efficiency organic solar cells, Org. Electron. 57 (2018) 239–246 https://doi.org/10.1016/j.orgel.2018.03.017.
[6] C. Dwivedi, T. Mohammad, V. Bharti, A. Patra, S. Pathak, V. Dutta, CoSP approach for the synthesis of blue MoO_3 nanoparticles for application as hole transport layer (HTL) in organic solar cells, Sol. Energy 162 (2018) 78–83 https://doi.org/10.1016/j.solener.2017.12.063.
[7] N. Chaturvedi, S.K. Swami, V. Dutta, Electric field assisted spray deposited MoO_3 thin films as a hole transport layer for organic solar cells, Sol. Energy 137 (2016) 379–384 https://doi.org/10.1016/j.solener.2016.08.038.
[8] R. Ji, J. Cheng, X. Yang, J. Yu L. Li, Enhanced charge carrier transport in spray-cast organic solar cells using solution processed MoO_3 micro arrays, RSC Adv. 7 (2017) 3059 https://doi.org/10.1039/C6RA27647D.
[9] D.M. Marathe, H.S. Tarkas, M.S. Mahajan, G.S. Lonkar, S.R. Tak, J.V. Sali, Bulk heterojunction thin film formation by single and dual feed ultrasonic spray method for application in organic solar cells, J. Semicond. 37 (2016) 093003https://doi.org/10.1088/1674-4926/37/9/093003.
[10] G. Prunet, L. Parrenin, E. Pavlopoulou, G. Pecastaings, C. Brochon, G. Hadziioannou, E. Cloutet, Aqueous PCDTBT:PC_{71}BM photovoltaic inks made by nanoprecipitation, Macromol. Rapid Commun. 39 (2018) 1700504 https://doi.org/10.1002/marc.201700504.
[11] W.C. Chang, D.H. Lan, K.M. Lee, X.F. Wang, C.L. Liu, Controlled deposition and performance optimization of perovskite solar cells using ultrasonic spray-coating of photoactive layers, ChemSusChem 10 (2017) 1405–1412 https://doi.org/10.1002/cssc.201601711.
[12] A.G. Macedo, D.C. Silva, N.A.D. Yamamoto, L. Micaroni, R.M.Q. Mello, L.S. Roman, Bilayer and bulk heterojunction solar cells with functional poly(2,2-bithiophene) films electrochemically deposited from aqueous emulsion, Synth. Met. 170 (2013) 63–68 https://doi.org/10.1016/j.synthmet.2013.02.019.
[13] N.A.D. Yamamoto, L.F. Lima, R.E. Perdomo, R. Valaski, V.L. Calil, A.G. Macedo, M. Cremona, L.S. Roman, Modification of PEDOT:PSS anode buffer layer with HFA for flexible polymer solar cells, Chem. Phys. Lett. 572 (2013) 73–77 https://doi.org/10.1016/j.cplett.2013.04.022.
[14] R.S. Edwards, K.S. Coleman, Graphene synthesis: relationship to applications, Nanoscale 5 (2013) 38–51 https://doi.org/10.1039/C2NR32629A.

[15] N.K. Elumalai, A. Saha, C. Vijila, R. Jose, Z. Jie, S. Ramakrishna, Enhancing the stability of polymer solar cells by improving the conductivity of the nanostructured MoO_3 hole-transport layer, Phys. Chem. Chem. Phys. 15 (2013) 6831–6841 https://doi.org/10.1039/C3CP50994J.

[16] C.P. Li, C.A. Wolden, A.C. Dillon, R.C. Tenent, Electrochromic films produced by ultrasonic spray deposition of tungsten oxide nanoparticles, Sol. Energy Mater. Sol. Cells 99 (2012) 50–55 https://doi.org/10.1016/j.solmat.2011.03.034.

[17] C. Girotto, B.P. Rand, S. Steudel, J. Genoe, P. Heremans, Nanoparticle-based, spray-coated silver top contacts for efficient polymer solar cells, Org. Electron. 10 (2009) 735–740 https://doi.org/10.1016/j.orgel.2009.03.006.

[18] V. Amendola, M. Meneghetti, What controls the composition and the structure of nanomaterials generated by laser ablation in liquid solution? Phys. Chem. Chem. Phys. 15 (2013) 3027–3046 https://doi.org/10.1039/C2CP42895D.

[19] D. Zhang, B. Gokce, S. Barcikowski, Laser synthesis and processing of colloids:fundamentals and applications, Chem. Rev. 117 (2017) 3990–4103 https://doi.org/10.1021/acs.chemrev.6b00468.

[20] J.F. Moulder, W.F. Stickle, P.E. Sobol, K.D. Bomben, Handbook of Photoelectron Spectroscopy, Physic. Electron. Corp., Eden Prairie, MN, 1992.

[21] D.J. Coutinho, R.M. Faria, Photocurrent in bulk heterojunction solar cells with similar electron and hole mean free path, Appl. Phys. Lett. 103 (2013) 223304 https://doi.org/10.1063/1.4834955.

[22] L.Q. Mai, B. Hu, W. Chen, Y.Y. Qi, C.S. Lao, R.S. Yang, Y. Dai, Z.L. Wang, Lithiated MoO_3 nanobelts with greatly improved performance for lithium batteries, Adv. Mater. 19 (21) (2007) 3712–3716 https://doi.org/10.1002/adma.200700883.

[23] M.T. Greiner, L. Chai, M.G. Helander, W.M. Tang, Z.H. Lu, Transition metal oxide work functions: the influence of cation oxidation state and oxygen vacancies, Adv. Funct. Mater. 22 (2012) 4557–4568 https://doi.org/10.1002/adfm.201200615.

[24] M. Vasilopoulou, A.M. Douvas, D.G. Georgiadou, L.C. Palilis, S. Kennou, L. Sygellou, A. Soultati, I. Kostis, G. Papadimitropoulos, D. Davazoglou, P. Argitis, The influence of hydrogenation and oxygen vacancies on molybdenum oxides work function and gap states for application in organic optoelectronics, J. Am. Chem. Soc. 134 (39) (2012) 16178–16187 https://doi.org/10.1021/ja3026906.

[25] G. Gershinsky, H.D. Yoo, Y. Gofer, D. Aurbach, Electrochemical and spectroscopic analysis of Mg2+ intercalation into thin film electrodes of layered oxides: V_2O_5 and MoO_3, Langmuir 29 (2013) 10964–10972 https://doi.org/10.1021/la402391f.

[26] S. Dayal, C.S. Kumar, Development of hierarchical layered nanostructured α-MoO_3 thin films using dc magnetron sputtering, Mater. Res. Express 3 (2016) 106405 https://doi.org/10.1088/2053-1591/3/10/106405.

[27] Y.O. Khyzhun, T. Strunskus, Y.M. Solonin, XES, XPS and NEXAFS studies of the electronic structure of cubic $MoO_{1.9}$ and $H_{1.63}MoO_3$ thick films, J. Alloy. Comp. 366 (1–2) (2004) 54–60 https://doi.org/10.1016/S0925-8388(03)00736-9.

[28] L.D. Lopez-Carreno, et al., Different oxidation states of polycrystalline molybdenum treated by O_2-plasma or O_2-ion bombardment, Surf. Sci. 402 (1998) 174–177 https://doi.org/10.1016/S0039-6028(97)00973-4.

[29] S.H. Lee, H. Nishi, T. Tatsuma, Tunable plasmon resonance of molybdenum oxide nanoparticles synthesized in non-aqueous media, Chem. Commun. 53 (94) (2017) 12680–12683 https://doi.org/10.1039/C7CC08090E.

[30] M.M.Y.A. Alsaif, M.R. Field, T. Daeneke, A.F. Chrimes, W. Zhang, B.J. Carey, K.J. Berean, S. Walia, J. van Embden, B. Zhang, K. Latham, K. Kalantar-zadeh, J.Z. Ou, Exfoliation solvent dependent plasmon resonances in two-dimensional sub-stoichiometric molybdenum oxide nanoflakes, ACS Appl. Mater. Interfaces 8 (5) (2016) 3482–3493 https://doi.org/10.1021/acsami.5b12076.

[31] Y.C. Liu, G.L. Griffin, S.S. Chan, I.E. Wachs, Photo-oxidation of methanol using MoO_3/TiO_2: catalyst structure and reaction selectivity, J. Catal. 94 (1985) 108–119 https://doi.org/10.1016/0021-9517(85)90086-7.

[32] I. Navas, R. Vinodkumar, V.P. Mahadevan Pillai, Self-assembly and photo-luminescence of molyddenum oxide nanoparticles, Appl. Phys. A 103 (2011) 373–380 https://doi.org/10.1007/s00339-011-6345-9.

[33] R.T. White, E.S. Thibau, Z.H. Lu, Interface structure of MoO_3 on organic semiconductors, Sci. Rep. 6 (2016) 21109 https://doi.org/10.1038/srep21109.

[34] R.A. Masitas, S.L. Allen, F.P. Zamborini, Size-dependent electrophoretic deposition of catalytic gold nanoparticles, J. Am. Chem. Soc. 138 (2016) 15295–15298 https://doi.org/10.1021/jacs.6b09172.

[35] S. Balendhran, S. Walia, M. Alsaif, E.P. Nguyen, J.Z. Ou, S. Zhuiykov, S. Sriram, M. Bhaskaran, K. Kalantar-zadeh, Field effect biosensing platform based on 2D αMoO_3, ACS Nano 7 (11) (2013) 9753–9760 https://doi.org/10.1021/nn403241f.

[36] C. Girotto, E. Voroshazi, D. Cheyns, P. Heremans, B.P. Rand, Solution-processed MoO_3 thin films as a hole-injection layer for organic solar cells, ACS Appl. Mater. Interfaces 3 (2011) 3244–3247 https://doi.org/10.1021/am200729k.

[37] S. Chambon, L. Derue, M. Lahaye, B. Pavageau, L. Hirsch, G. Wantz, MoO_3 Thickness, Thermal annealing and solvent annealing effects on inverted and direct polymer photovoltaic solar cells, Materials 5 (2012) 2521–2536 https://doi.org/10.3390/ma5122521.

[38] B. Kannan, R. Pandeeswari, B.G. Jeyaprakash, Influence of precursor solution volume on the properties of spray deposited α-MoO_3 thin films, Ceram. Int. 40 (2014) 5817–5823 https://doi.org/10.1016/j.ceramint.2013.11.022.

[39] A.K. Prasad, P.I. Goumaa, D.J. Kubinski, J.H. Visser, R.E. Soltis, P.J. Schmitz, Reactively sputtered MoO_3 films for ammonia sensing, Thin Solid Films 436 (2003) 46–51 https://doi.org/10.1016/S0040-6090(03)00524-8.

[40] K. Galatsis, Y.X. Lia, W. Wlodarski, E. Comini, G. Faglia, G. Sberveglieri, Semiconductor MoO_3–TiO_2 thin film gas sensors, Sensor. Actuator. B 77 (2001) 472–477 https://doi.org/10.1016/S0925-4005(01)00737-7.

[41] W. Zeng, K.S. Yong, Z.M. Kama, Z.K. Chen, Y. Li, Effect of MoO_3 as an interlayer on the performance of organic solar cells based on ZnPc and C_{60}, Synth. Met. 161 (2012) 2748–2752 https://doi.org/10.1016/j.synthmet.2011.10.014.

[42] M. Kröger, S. Hamwi, J. Meyer, T. Riedl, W. Kowalsky, A. Kahn, Role of the deep-lying electronic states of in the enhancement of hole-injection in organic thin films, Appl. Phys. Lett. 95 (2009) 123301 https://doi.org/10.1063/1.3231928.

[43] J. Meyer, A. Shu, M. Kröger, A. Kahn, Effect of contamination on the electronic structure and hole-injection properties of semiconductor interfaces, Appl. Phys. Lett. 96 (2010) 133308 https://doi.org/10.1063/1.3374333.

[44] J. Meyer, R. Khalandovsky, P. Görrn, A. Kahn, MoO_3 films spin-coated from a nanoparticle suspension for efficient hole-injection in organic electronics, Adv. Mater. 23 (2011) 70–73 https://doi.org/10.1002/adma.201003065.

[45] W. Ma, C. Yang, X. Gong, K. Lee, A.J. Heeger, Thermally stable, efficient polymer solar cells with nanoscale control of the interpenetrating network morphology, Adv. Funct. Mater. 15 (2005) 1617–1622 https://doi.org/10.1002/adfm.200500211.

[46] M.F. Xu, L.S. Cui, X.Z. Zhu, C.H. Gao, X.B. Shi, Z.M. Jin, Z.K. Wang, L.S. Liao, Aqueous solution-processed MoO_3 as an effective interfacial layer in polymer/fullerene based organic solar cells, Org. Electron. 14 (2013) 657–664 https://doi.org/10.1016/j.orgel.2012.12.016.

[47] B. Xu, S.A. Gopalan, A.I. Gopalan, N. Muthuchamy, K.P. Lee, J.S. Lee, Y. Jiang, S.W. Lee, S.W. Kim, J.S. Kim, H.M. Jeong, J.B. Kwon, J.H. Bae, S.W. Kang, Functional solid additive modified PEDOT:PSS as an anode buffer layer for enhanced photovoltaic performance and stability in polymer solar cells, Sci. Rep. 7 (2017) 45079 https://doi.org/10.1038/srep45079.

[48] M. Hermenau, M. Riede, K. Leo, S.A. Gevorgyan, F.C. Krebs, K. Norrman, Water and oxygen induced degradation of small molecule organic solar cells, Sol. Energy Mater. Sol. Cells 95 (2011) 1268–1277 https://doi.org/10.1016/j.solmat.2011.01.001.

[49] J. Subbiah, P.M. Beaujuge, K.R. Choudhury, S. Ellinger, F. So, Combined effects of MoO_3 interlayer and $PC_{70}BM$ on polymer photovoltaic device performance, Org. Electron. 11 (2010) 955–958 https://doi.org/10.1016/j.orgel.2010.02.006.